Engineering Research Journal
journal homepage: https://erj.journals.ekb.eg/

# Experimental Investigation of the In-Plane Cyclic Behavior of Hybrid GFRP-Steel Reinforced Squat Shear Walls

Mohamed Saad [1,*], Osama Amer [2], Ahmed H. Ali [1], Hisham Haggag [1]

[1] Helwan University - Faculty of Engineering - Department of Civil Engineering - Egypt
[2] Ain Shams University - Faculty of Engineering - Department of Civil Engineering – Egypt

[*]Corresponding author E-mail: mohamedD01275@m-eng.helwan.edu.eg

**Abstract.** The susceptibility of steel reinforcement to corrosion undermines the durability of reinforced concrete (RC) elements in aggressive environments. Glass Fiber Reinforced Polymer (GFRP) bars, with superior corrosion resistance and strength-to-weight efficiency, emerge as an optimal substitute. Yet, their cyclic seismic performance remains insufficiently examined. This research investigates the hysteretic behavior of squat GFRP-RC shear walls, hybrid GFRP-steel, and traditional steel bars. Six full-scale wall specimens—two GFRP-reinforced, two hybrid GFRP-steel, and two steel-reinforced controls—underwent quasi-static cyclic lateral loading. Hybrid GFRP-steel walls demonstrated hysteretic stability with negligible residual drift, augmented by boundary elements which significantly bolstered lateral strength and mitigated residual deformations. Furthermore, these walls surpassed their GFRP-only counterparts in energy dissipation efficacy and deformation adaptability, underscoring their advanced seismic resilience in corrosive settings and the critical structural role of boundary elements. This study provides pivotal experimental insights, advocating the integration of GFRP as a viable replacement for steel reinforcement in seismic design, particularly in contexts where corrosion resistance is paramount.

**Keywords:** Reinforced concrete, Seismic performance, Cyclic in-plane test, RC squat shear wall, Glass Fibre-Reinforced Polymer (GFRP) bars

## 1 Introduction

The seismic performance RC shear walls has become a critical focus in earthquake engineering, given their essential role in resisting lateral loads and preserving structural integrity under seismic stress. As primary lateral-load-resisting components in seismic-resistant structures, RC shear walls substantially contribute to lateral stiffness, strength, and resilience, particularly in regions of high seismic activity [1]. Within the spectrum of shear wall designs, squat shear walls—characterized by low height-to-length ratios—are extensively used in low-rise buildings, industrial facilities, and bridge substructures where

DOI: 10.21608/erj.2025.341951.1154
Received 08 December 2024; Received in revised form 02 January 2025; Accepted 03 January 2025
Available online 01 March 2025

architectural or operational constraints limit height [2-4]. While squat walls offer substantial lateral stiffness, their low aspect ratios render them vulnerable to shear-dominated failure mechanisms under cyclic loads, common during seismic events [5,6]. Addressing these vulnerabilities, particularly regarding shear capacity and failure modes, is essential to optimizing their seismic performance.

Traditionally, steel reinforcement has been the preferred choice for RC shear walls in earthquake-resistant design due to its well-documented ductility, energy dissipation capabilities, and robustness under cyclic loading [7,8]. However, steel's inherent susceptibility to corrosion—exacerbated in environments with moisture, chloride exposure, or other corrosive agents—compromises long-term durability and incurs substantial repair costs, impacting both structural safety and lifecycle costs [9-12]. In response, GFRP bars have emerged as a promising alternative, offering excellent corrosion resistance, a high strength-to-weight ratio, and durability in harsh environments, such as marine and coastal areas where steel would deteriorate rapidly [13]. Although GFRP's linear-elastic behavior presents challenges with regard to ductility, it also introduces potential advantages in seismic applications, including self-centering and reduced residual deformations post-event [14-20].

Despite these advantages, the seismic behavior of GFRP-reinforced shear walls—especially squat configurations—remains underexplored, as GFRP's unique mechanical properties diverge from those of steel. Its lack of yielding, coupled with linear-elastic characteristics, necessitates a reassessment of its seismic performance, as existing design provisions for steel-reinforced systems inadequately address GFRP-specific behaviors and could yield unreliable or unsafe predictions [21,22]. Studies suggest that while GFRP-reinforced RC walls achieve satisfactory drift capacities and stable hysteretic responses, their energy dissipation and post-cracking stiffness fall below those of steel-reinforced walls [8,19,23,24]. Furthermore, incorporating boundary elements is crucial in GFRP-reinforced systems to enhance shear strength, particularly for mitigating shear-dominated failures such as diagonal tension and shear-compression [3, 25].

Seismic performance in squat shear walls is governed by complex interactions among design parameters, including aspect ratio ($\alpha_s$), reinforcement configuration, boundary elements, and axial load ratios. Low aspect ratios yield high shear strengths but can limit ductility, making walls susceptible to brittle, shear-dominated failure under seismic stress [3]. The configuration of web reinforcement is key in controlling crack propagation, enhancing post-cracking stiffness, and delaying shear failure [20,26]. Boundary elements, which confine compression zones, improve shear capacity by bolstering concrete strength and modifying the strut geometry, especially under higher axial loads [27,28]. Understanding these interactions is critical to optimizing squat shear walls reinforced with GFRP, whose cyclic response diverges notably from steel.

Addressing these challenges, this study expands the current knowledge on the seismic response of GFRP-reinforced squat shear walls. Through an experimental program on six full-scale RC squat shear walls—reinforced with steel, GFRP, or hybrid systems—this research highlight the implications of reinforcement type, vertical reinforcement ratios, and boundary elements on key seismic performance metrics, including strength, stiffness degradation, and failure mechanisms under reversed cyclic loading. This study delivers a comparative evaluation of steel and GFRP reinforcement systems, providing acumen into the distinct strengths and constraints of each approach. The findings offer foundational guidance for the development of robust design provisions tailored to GFRP-reinforced shear walls, with important implications for improving the durability and resilience of RC structures in seismically active regions.

## 2 Material And Methods

This study investigates the in-plane cyclic behaviour of RC squat shear walls reinforced with hybrid GFRP/steel systems, juxtaposed with walls reinforced exclusively with either conventional steel or GFRP bars. The experimental investigation encompasses testing six full-scale RC squat shear wall,

categorized based on reinforcement configurations. Two principal configurations are analyzed: walls featuring distributed vertical reinforcement across the web and walls incorporating boundary elements with vertical reinforcement concentrated at the extremities. Each specimen was tested under quasi-static reversed cyclic lateral loading to simulate seismic forces, and their structural response was assessed with reference to strength, stiffness degradation, ductility, and failure mechanisms.

With $\alpha_s$ of 1.2, all specimens were designed to meet the seismic-force resisting system (SFRS) requirements stipulated in ACI 318 [29] and ECP 203 [30]. Two specimen categories were defined: Category A (SW1, SGW1, GW1) with uniformly distributed vertical reinforcement, and Category B (SW2, SGW2, GW2) incorporating boundary elements to increase end wall reinforcement. This categorization enabled a focused assessment of the influence of boundary elements on the shear behavior of GFRP-RC walls, particularly in mitigating shear-induced failures. Table 1 outlines the reinforcement details, while Fig. 1 and 2 present the corresponding wall configurations.

**Table 1.** Geometrical properties and reinforcement details of tested walls

| Wall | Dimensions | | | | Vertical reinforcement | | | | Horizontal reinforcement | |
|---|---|---|---|---|---|---|---|---|---|---|
| | $l_w$ mm | $l_a$ mm | $t_w$ mm | $h_w$ mm | No. & size | $\rho_V$ (%) $\rho_{V-st}$ (%) | $\rho_{V-GFRP}$ (%) | $\rho_{V-total}$ (%) | No. & size | $\rho_H$ (%) |
| SW1 | 1500 | - | 150 | 1800 | 12T12+2×3T12a | 0.90 | - | 0.90 | T8b@ 167 mm | 0.40 |
| SGW1 | | - | | | 26F3c + 2×3T12 | 0.20 | 1.04 | 1.24 | T8@ 167 mm | 0.40 |
| GW1 | | - | | | 24F3+2×8F3 | - | 1.60 | 1.60 | F3@ 100 mm | 1.20 |
| SW2 | | 250 | | | 8T12+2×6T12 | 1.01 | - | 1.01 | T8@ 167 mm | 0.40 |
| SGW2 | | 250 | | | 20F3 + 2×6T12 | 0.60 | 0.80 | 1.40 | T8@ 167 mm | 0.40 |
| GW2 | | 250 | | | 20F3+2×14F3 | - | 1.92 | 1.92 | F3@ 100 mm | 1.20 |

Note: [a]Steel bars $d_b = 12mm$; [b]Steel bars $d_b = 8mm$; [c]GFRP bars No. 3.; $l_w$ Wall length; $l_a$ Boundary zone length; $t_w$ *Wall thickness*; $h_w$ Wall height; $\rho_{V-GFRP}$ Vertical/longitudinal GFRP reinforcement ratio; $\rho_{V-st}$ Vertical/longitudinal steel reinforcement ratio; $\rho_{V-total}$ Total vertical/longitudinal reinforcement ratio; $\rho_H$ horizontal reinforcement ratio.

All walls specimen measured 1800 mm in height, 1500 mm in length, and 150 mm in thickness—dimensions representative of typical squat shear wall geometries in practice. For Category B walls, boundary elements measuring 250 mm in length were added. All specimens were anchored to a RC footing measuring 2500 mm (length), 500 mm (width), and 500 mm (depth). Designed as an RC rigid foundation, the footing, heavily reinforced with 18M Grade 60 steel bars, provided anchorage for the longitudinal reinforcement, minimized base deformations, reducing excessive cracking and premature base failures to ensure unaltered cyclic load responses.

To prevent out-of-plane displacements and ensure stability under inelastic deformations, double-layer vertical reinforcement was adopted for all tested to ensure stability under inelastic deformations, following guidelines by Paulay and Priestley [2] and El-Azizy et al. [31]. Wall designs adhered to the provisions of ECP 203 [30] and ACI 318 [29] for steel reinforced walls, besides ECP 208 [32] and ACI 440 [33] for GFRP-reinforced walls, ensuring that the specimens would develop shear failure prior to flexural failure. This design consideration allowed for an in-depth investigation of shear behavior.

A consistent normal-weight concrete mix with a targeted compressive strength $(f_{cu})$ of $30MPa$ was utilized for all specimens. Key mix proportions included a 0.4 water-to-cement ratio, with water and cement contents of 160 kg/m³ and 400 kg/m³, respectively. The aggregate content was 1700 kg/m³, with a nominal maximum size of $10mm$. Compressive strength for every specimen was assessed through pre-test cylinder testing, conducted one day prior to loading; detailed results are presented in Table 2.

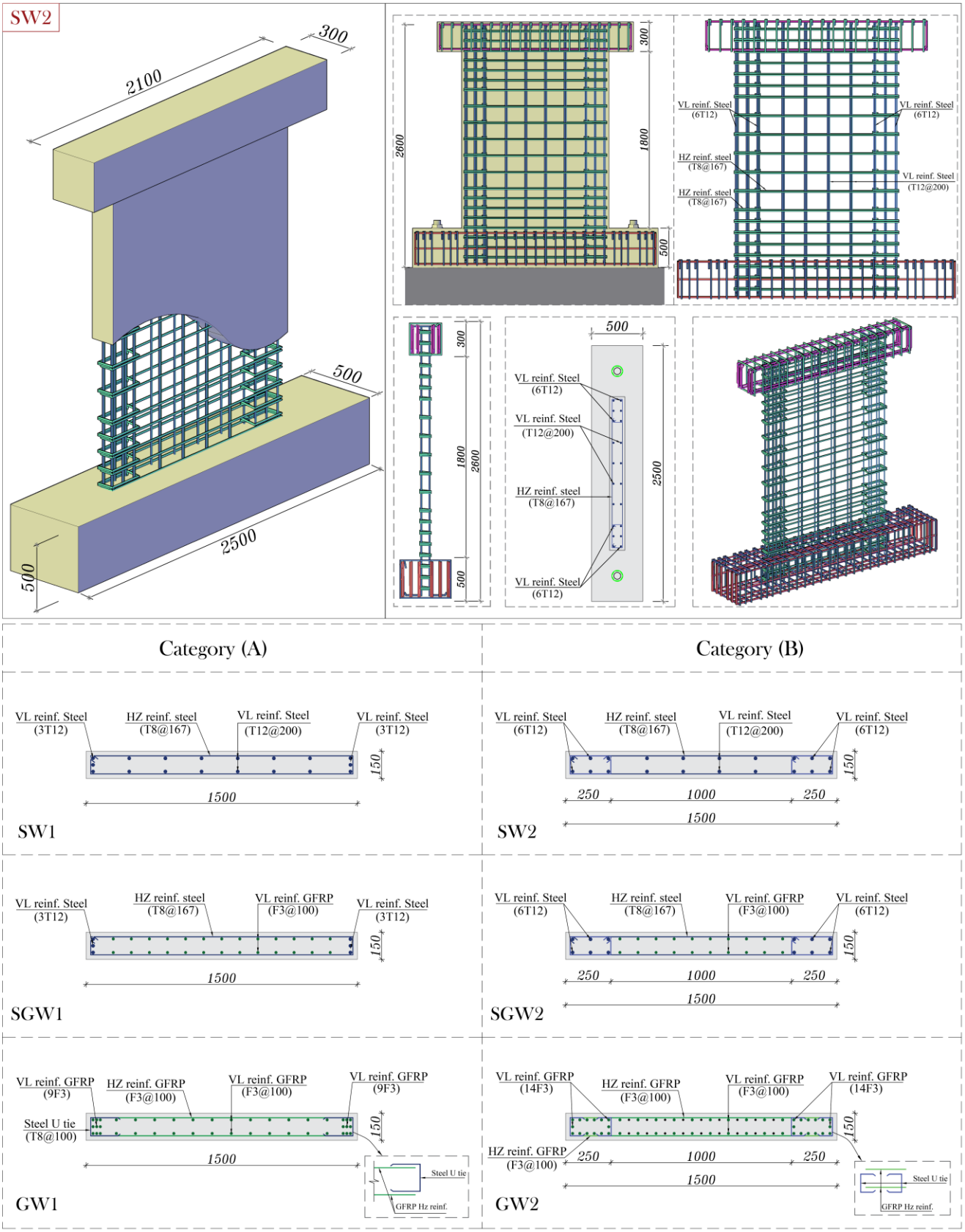


**Fig. 1.** Concrete dimensions and Reinforcement configuration details for all tested walls (dimensions in mm)

The average concrete tensile strength ($f_{ctr}$) and elasticity modulus ($E$) were computed using the relations $E = 4400\sqrt{f_{cu}}$ and $f_{ctr} = 0.6\sqrt{f_{cu}}$, in line with ECP 203 [30]. Consistent concrete properties across all specimens ensured comparability of results.

For reinforcement, steel-RC walls (SW1 and SW2) utilized grade 400/600 steel bars for vertical/longitudinal reinforcement and Grade 240/360 steel bars for horizontal/transverse reinforcement. Hybrid-RC walls (SGW1 and SGW2) incorporated longitudinal bars with grade 400/600 in the boundary elements. GFRP-RC walls (GW1 and GW2) employed, for both longitudinal and transverse reinforcement, sand-coated high-modulus GFRP bars. Transverse reinforcement comprised #3 GFRP bars, spaced at $100mm$. U-shaped 8 mm steel stirrups were placed at the ends to prevent bending failures in the GFRP bars. Vertical web reinforcement was configured to meet target reinforcement ratio, as detailed in Table 1. GFRP bar mechanical properties were validated following ASTM-D7205 [34] and are summarized in Table 2. The GFRP bars used for reinforcement were manufactured with a fiber volume fraction (FVF) of 70%, as provided by the manufacturer. This high FVF is critical for achieving the desired mechanical properties, including a tensile strength ($f_{fu}$) of 880 MPa and an elastic modulus ($E_f$) of 53.4 GPa (Table 2). The sand-coated surface of the bars ensured adequate bond performance with the surrounding concrete, crucial for maintaining shear transfer across cracks.

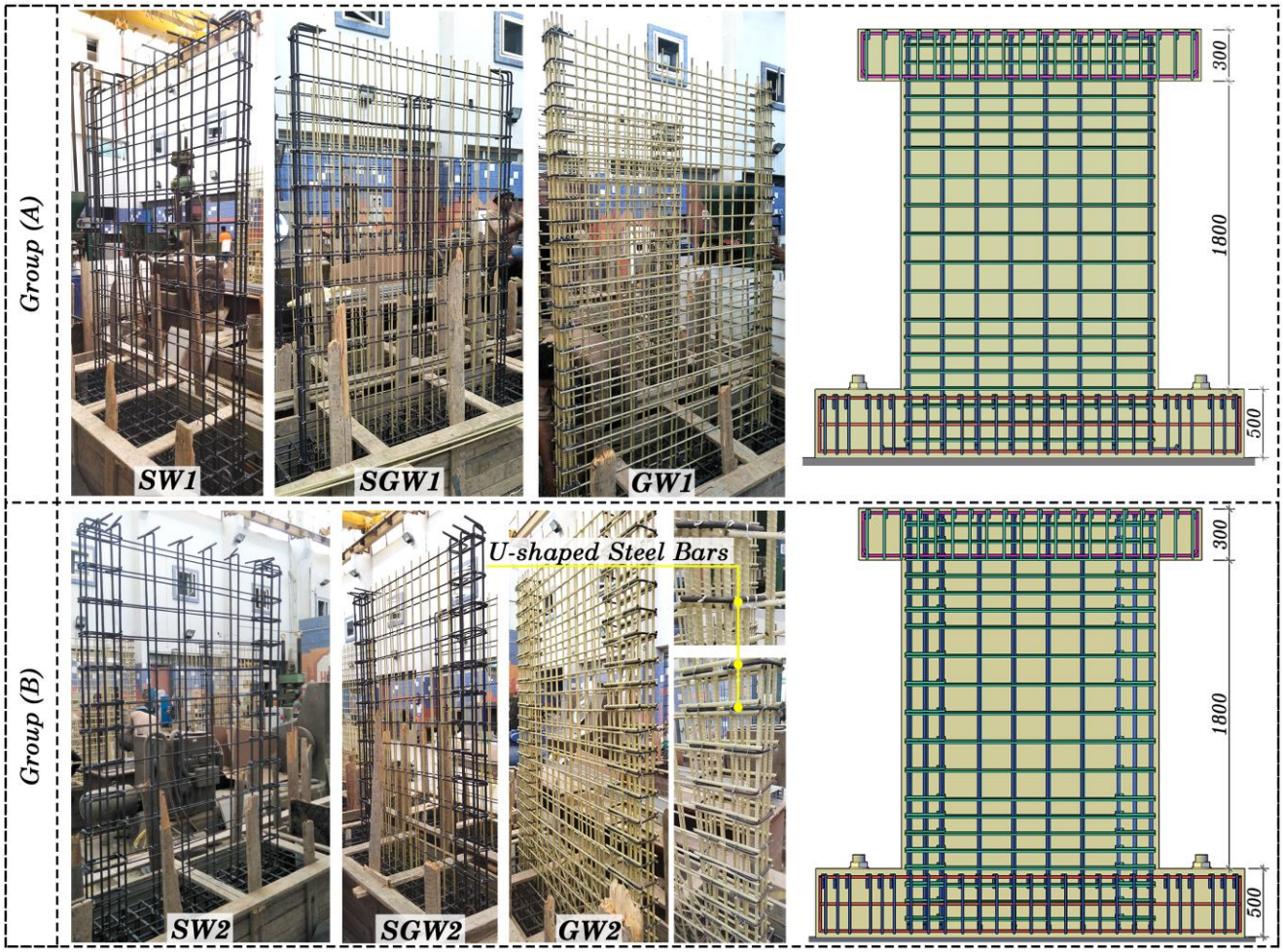


**Fig. 2.** Reinforcement configuration of steel, hybrid GFRP-steel, and GFRP reinforced walls

A servo-controlled hydraulic actuator, featuring a ±250 mm stroke and a ±1300 kN capacity, was employed to impose the lateral quasi-static cyclic loading. This actuator, fixed to a rigid reaction frame,

was coupled with a top RC cap beam, facilitating uniform load transfer across the tested specimens (Fig. 3a). The applied loading protocol, shown in Fig. 3b, comprised two fully-reversed lateral displacement cycles to emulate seismic loading conditions. A comprehensive instrumentation array, including LVDTs, was deployed for the measurement of key response parameters, including axial deformations, lateral displacements, base sliding, and concrete strains.

**Table 2.** Material properties of employed concrete and reinforcements systems

| | | | | | |
|---|---|---|---|---|---|
| Concrete (C30) | $W/C$ (%) | $Cement\ (Kg/m^3)$ | $E_c(GPa)$ | $f_{cu}(MPa)$ | C.O.V. (%) |
| | 0.4 | 400 | 24.1 | 32.4 | 5.5 |
| Steel bars | $d_b(mm)$ | $A_s(mm^2)$ | $E_s(GPa)$ | $f_y(MPa)$ | $\varepsilon_y$(%) |
| | 8 | 50.3 | 200 | 240 | 0.2 |
| | 12 | 113 | | 400 | |
| GFRP bars #3 | $d_b(mm)$ | $A_f(mm^2)$ | $E_f(GPa)$ | $f_{fu}(MPa)$ | $\varepsilon_{fu}$(%) |
| | 9.53 | 71.33 | 53.4 | 880 | 2.0 |

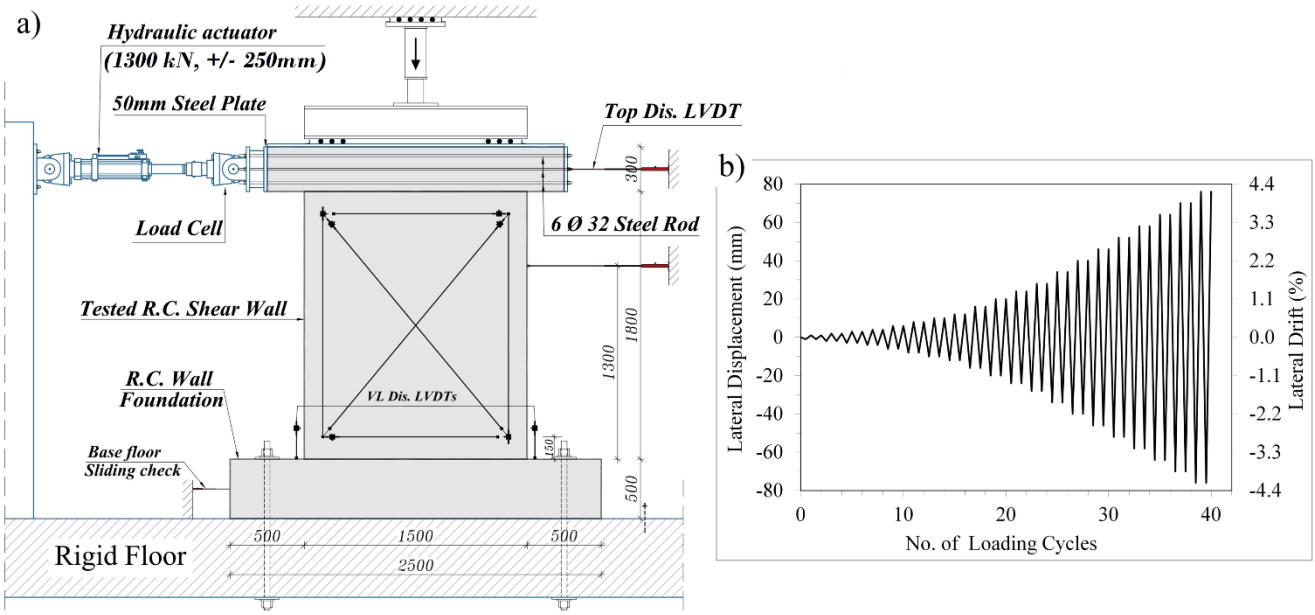


**Fig. 3.** Test setup layout (a) and displacement-controlled loading protocol (b)

## 3 Results and discussions

Reversed cyclic lateral loading tests yielded key insights into the role of reinforcement (type and ratio), along with the inclusion of boundary zones, influenced their overall seismic performance. This section presents a detailed analysis of the experimental outcomes, focusing on damage propagation, crack patterns, in-plane lateral resistance, displacement capacity, hysteresis response, stiffness degradation, fundamental period shifts, and ductility. Comparative appraisal of the different reinforcement configurations—steel, GFRP, and hybrid systems—elucidates the critical role of these key design parameters in defining the response of GFRP-RC squat walls during seismic events.

### 3.1 Backbone curves

The backbone curves, derived from the load-displacement and moment-rotation responses, offer essential insights into the cyclic response of the tested walls. As depicted in Fig. 4, in the pre-cracking

phase, all walls displayed similar initial slopes, reflecting the elastic performance of concrete and reinforcement. However, with increasing loads, distinct differences in stiffness emerged, predominantly influenced by the type and configuration of reinforcement used.

Vertical loads enhance the shear resistance of reinforced concrete squat walls by increasing the compression in the diagonal struts formed within the wall under cyclic lateral loads. This axial compression delays the initiation of diagonal tension cracks and mitigates their propagation, thereby improving the overall seismic performance of the walls. However, excessive axial loads could lead to premature crushing of the concrete or buckling of the longitudinal reinforcement. For all tested walls, the applied vertical load ratios were designed to reflect realistic conditions, ensuring that the failure mechanisms observed were representative of practical seismic scenarios.

Steel-RC walls exhibited higher stiffness in the initial stages of loading, attributable to the superior elastic modulus of steel. Following steel yielding, a pronounced stiffness reduction occurred, reflecting ductile behaviour that facilitated substantial energy absorption along with progressive stiffness degradation—aligning with anticipated seismic response characteristics of steel-RC systems. In contrast, GFRP-RC walls showed lower initial stiffness due to GFRP's lower elastic modulus. However, the linear-elastic nature of GFRP contributed to consistent stiffness retention throughout the loading progress, as the material continued to strain-harden without yielding, a response documented in prior researches [28, 35].

Hybrid-RC walls demonstrated intermediate stiffness characteristics, benefiting from the ductility of steel and the elastic resilience of GFRP. This combination provided enhanced and slower stiffness degradation compared to GFRP-only walls, aligning with research on hybrid reinforcement systems [8,13,23,24].

The inclusion of boundary confinement significantly influenced seismic response. In SW2 and GW2, boundary elements delayed concrete crushing, increasing peak load and deformation capacity before failure. For GFRP walls, boundary elements mitigated the brittle nature of GFRP, enhancing strength and deformation capacity, underscoring their importance in seismic design.

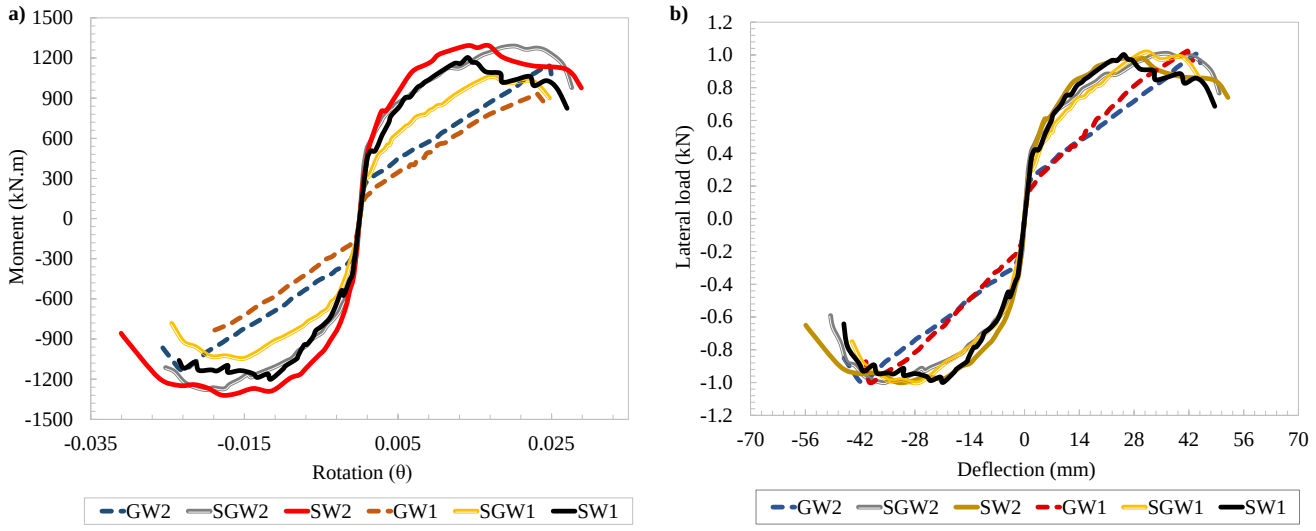


**Fig. 4.** Envelope curves of test walls: a) moment-rotation envelope curves, and b) normalized load-displacement envelope curves

## 3.2 Damage propagation and plastic hinge formation

Damage progression and plastic hinge formation were significantly dictated by the reinforcement set and the incorporation of boundary confinement. Fig. 5 and Fig. 6 delineate the final crack topology and characteristic failure modes for the tested walls with uniform reinforcement (Group A) and those with

boundary elements (Group B). This section offers a rigorous analysis of crack propagation, failure mechanisms, and plastic hinge development, elucidating the contribution of different reinforcement types—steel, GFRP, and hybrid systems—on the seismic performance of the walls.

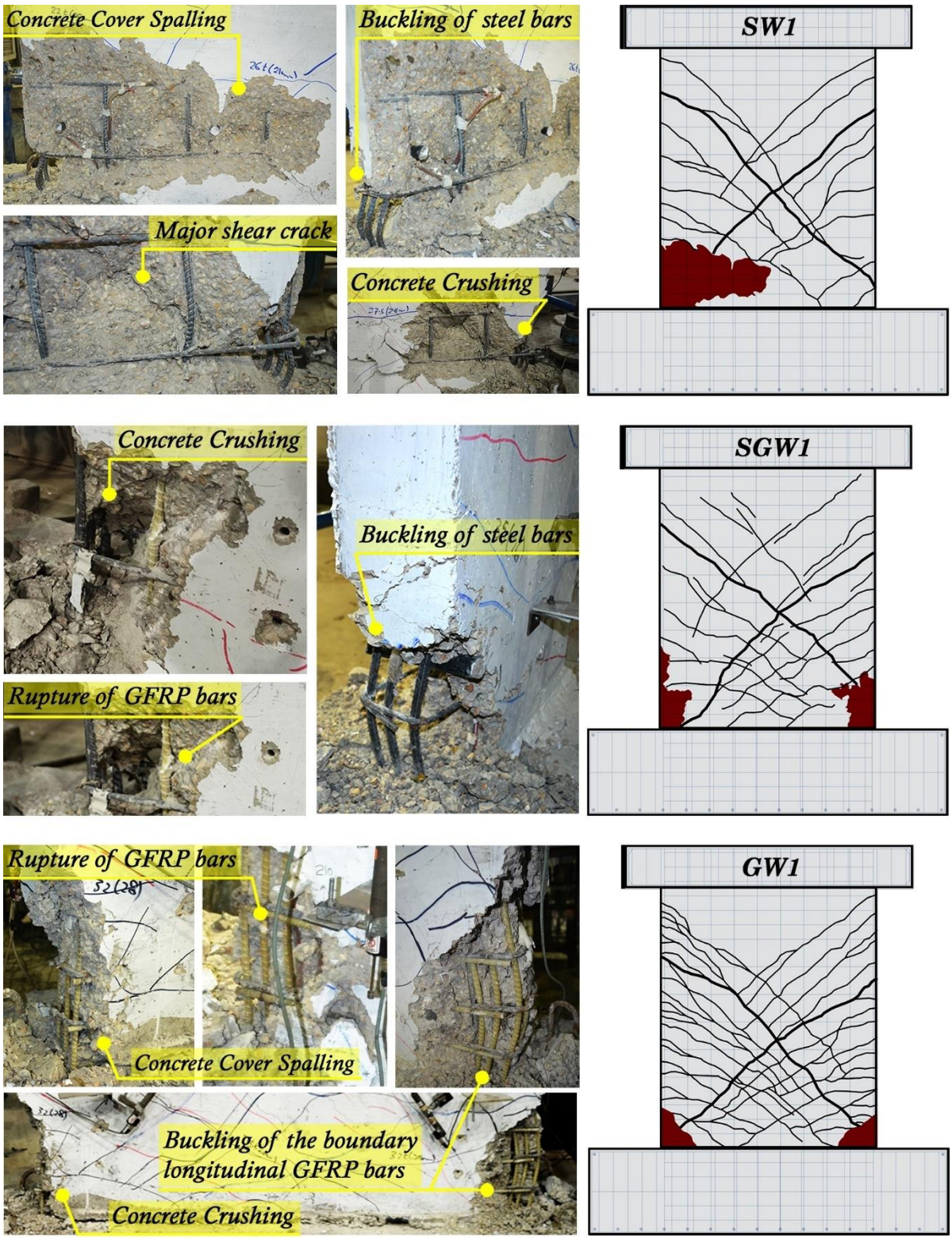


**Fig. 5.** Crack patterns and damage observed at failure of walls SW1, SGW1 and GW1

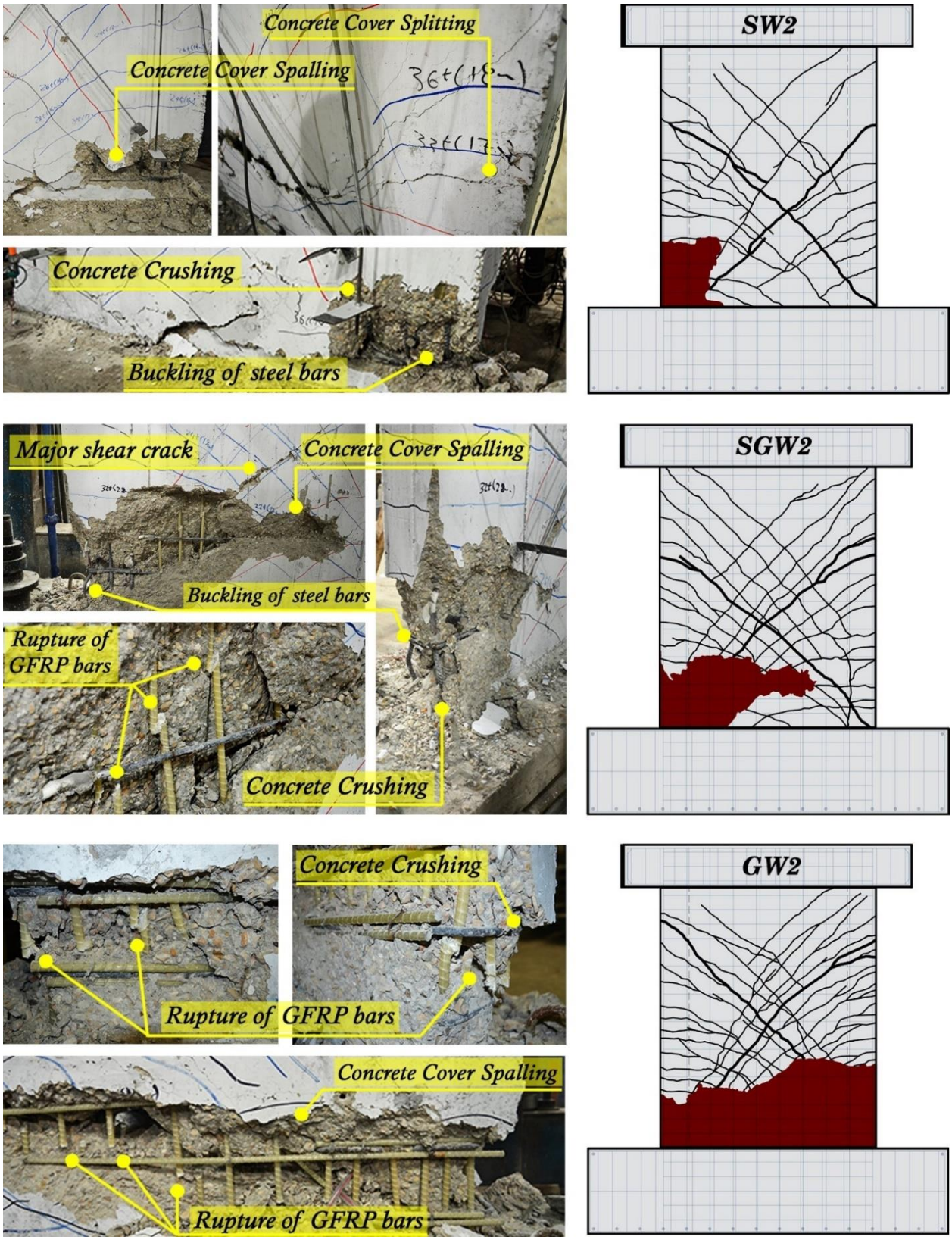


**Fig. 6.** Crack patterns and damage observed at failure of walls SW2, SGW2 and GW2

### Steel-Reinforced Walls

Steel-RC walls demonstrated typical flexural-shear cracking behaviors commonly observed in RC structures subjected to cyclic loading. Vertical splitting cracks nucleated at the walls' compression ends

when concrete strain reached approximately 0.003 to 0.0035. Diagonal cracks formed near the wall toes, propagating upward toward the compression zone and steepening under increased lateral loads. As drift levels rose to 0.14% in SW1 and 0.18% in SW2, additional shear cracks developed near the upper regions of the walls, with SW2 displaying steeper crack angles stemming from the confining effects of boundary confinement. These boundary elements significantly influenced the width and inclination of the cracks near the wall edges, delaying severe damage and restricting crack propagation within the compression zone. As the loading increased, concrete spalling intensified, particularly near the base, where longitudinal bar buckling was observed. Plastic hinge formation was localized at the base, facilitated by the inelastic elongation capacity of the reinforcement steel, resulting in concentrated plastic deformation. This ductile response is characteristic of steel-RC walls, wherein plastic hinges develop in the lower regions and progressively evolve under increasing load levels [2].

**GFRP-Reinforced Walls**

GFRP-RC walls exhibited a more distributed cracking pattern. Initial flexural cracks were followed by finer shear cracks propagating throughout the web, indicating a less localized response than observed in steel-reinforced walls. The initial shear cracks extended toward the upper wall regions, steepening as the drift increased to 0.29% in GW1 and 0.36% in GW2. Vertical splitting cracks appeared at the highly compressed fibers of the boundary elements, and shear cracks within the compression zone became increasingly prominent at higher drift levels (1.31% for GW1 and 1.43% for GW2). The distinct cracking behavior of walls GW1 and GW2 was influenced by the high fiber volume fraction (FVF) of the bars, which facilitated efficient stress transfer between the fibers and the matrix, preventing localized stress concentrations. As a result, GW2, which incorporated boundary elements, exhibited enhanced shear resistance and delayed diagonal compression failures compared to GW1. The linear-elastic behavior of the GFRP bars ensured that the walls retained stiffness even at higher drift levels, albeit with reduced energy dissipation capacity compared to their steel-reinforced counterparts.

As the applied load increased, concrete spalling originated at the wall toes, signaling the onset of inelastic behavior. Unlike steel-reinforced walls, GFRP-reinforced walls did not exhibit a distinct yield point in the longitudinal reinforcement; plastic hinge formation was instead characterized by progressive spalling and the strain hardening behaviors of the GFRP bars. Ultimately, concrete failure manifested through the crushing of diagonal struts within the compression zone, confirming the predominance of the diagonal compression strut mechanism in shear force transfer. The inclusion of boundary confinement in GW2 slightly delayed the onset of crushing, facilitating marginally enhanced drift aptitude and underscoring the importance of confinement in optimizing the behaviour of GFRP-RC walls.

**Hybrid-Reinforced Walls**

The hybrid-RC walls displayed an intermediate behavior, incorporating characteristics from both steel- and GFRP-reinforcement systems. Diagonal shear cracks initiated at drift levels of 0.15% in SGW1 and 0.20% in SGW2, with patterns resembling those observed in steel-reinforced walls. However, the response was more gradual as a consequence of the strain-hardening performance of the GFRP bars. As loading amplitude increased, additional shear cracks developed, extending toward the compression zone and intersecting near-vertical cracks, creating a crisscross pattern that governed the walls' behavior. Vertical splitting cracks developed at heavily compressed fibers in the boundary elements in SGW2, mirroring the failure modes in GFRP-RC walls. Conversely, in SGW1—lacking boundary elements—the cracks remained inclined and more localized, leading to shear failure akin to that observed in SW1. However, SGW1 experienced less pronounced sliding shear displacements than SW1, indicating the efficacy of GFRP bars in mitigating sliding shear effects. The incorporation of boundary confinement in SGW2 facilitated a more ductile failure mechanism, characterized by gradual strength reduction and increased drift capacity, highlighting the synergistic benefits of steel- and GFRP-reinforcement in optimizing overall seismic performance [13,23].

### Plastic Hinge Formation

Plastic hinge formation varied significantly among the reinforcement types. In steel-reinforced walls, plastic hinges concentrated near the base, where the high inelastic elongation capacity of steel facilitated significant plastic deformation within a confined region. Primary cracks localized plasticity, yielding shorter plastic hinge lengths. Conversely, GFRP-RC walls experienced a more distributed plastic hinge formation attributable to the elastic characteristics of GFRP bars, leading to increased plastic hinge heights and localized compression strains in the heavily compressed zones. In hybrid-reinforced walls, plastic hinge formation combined the behaviors observed in both steel- and GFRP-RC walls. Steel yielding occurred near the boundary elements, concentrating plastic deformation, while GFRP bars in the web contributed to a more distributed inelastic response, extending the plastic hinge zone. The higher vertical reinforcement ratios in hybrid walls also facilitated additional flexural and diagonal shear cracks, redistributing tensile stresses over a larger area and spreading plasticity across an extended zone. The inclusion of boundary confinement further influenced plastic hinge formation, particularly in GFRP- and hybrid-RC walls. In GW2 and SGW2, boundary elements delayed concrete crushing, improved ability of diagonal struts to withstand compression, and facilitated higher drift capacities. This emphasizes the essential role of confinement in augmenting the ability of GFRP-RC systems to withstand seismic events, which tend to exhibit more brittle behavior without adequate confinement [28,35-37].

## 3.3 Hysteretic stiffness and fundamental period shift

### Stiffness Degradation

The cyclic response of the examined walls revealed a clear pattern of stiffness attenuation, reflecting the damage accumulation under cyclic loading. Quantitative assessment utilized normalized effective secant stiffness ($K_{nor} = K_{s,i}/K_{init}$) measurements across incremental drift ratios, where $K_{init}$ represents initial elastic stiffness derived from the primary load increment, and $K_{s,i}$ denotes the effective secant stiffness computed from the load-displacement curve slope at subsequent drift levels. The degradation of $K_{nor}$ across ascending drift levels is plotted in Fig. 7.

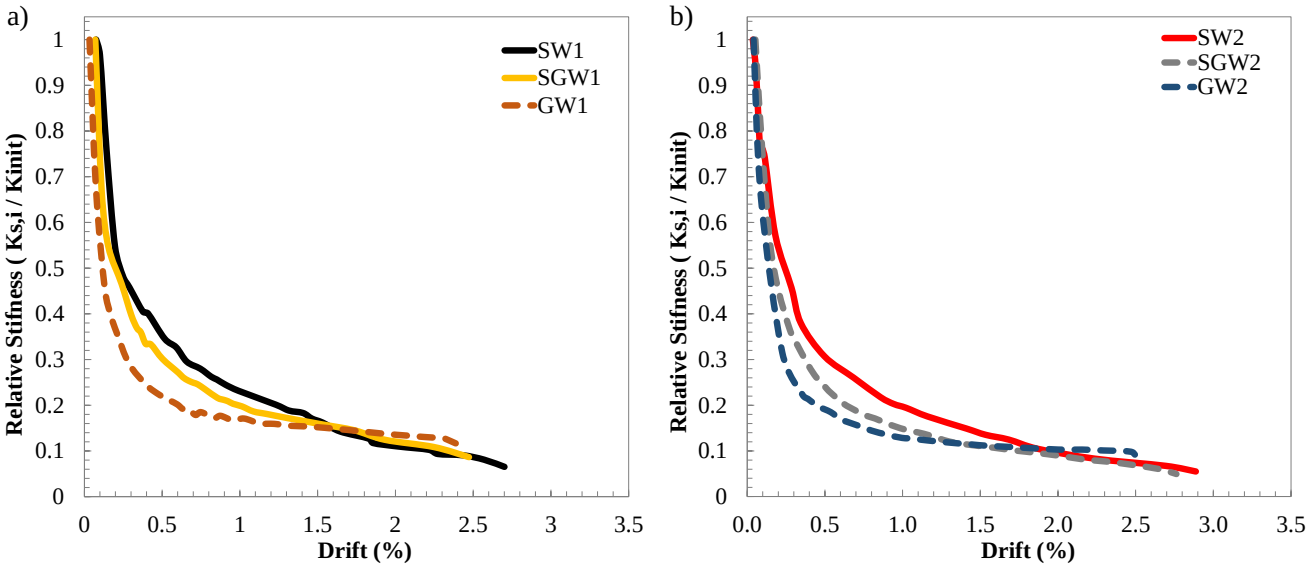


**Fig. 7.** Normalized stiffness degradation as a function of drift levels for a) uniform reinforcement configurations (Group A) and b) walls incorporating boundary elements (Group B)

While all walls followed a similar degradation trend, the rate and extent varied according to the reinforcement type. Steel-RC walls exhibited the most rapid and pronounced stiffness loss. Following the onset of steel yielding, their normalized stiffness dropped sharply, reaching approximately 5.4% and 6.5% of $K_{init}$ at failure for SW1 and SW2, respectively. This rapid degradation is a consequence to the steel yielding and the consequent formation of a plastic hinge at the wall base, resulting in pronounced stiffness reduction.

Conversely, GFRP-RC walls displayed superior stiffness retention relative to their steel-reinforced counterparts. The normalized stiffness for GW1 and GW2 remained above 12% at 1% drift and gradually decreased to 11.6% and 9.2% at failure. This behavior is ascribed to the elasticity characteristics of GFRP bars that, unlike steel, do not yield and thus maintaining the wall stiffness even at elevated drift levels. The strain-hardening effect of GFRP further mitigates the substantial stiffness attenuation typical in steel-reinforced walls, as corroborated by prior studies [8,21,24,28,38].

Hybrid-RC walls demonstrated intermediate stiffness degradation profile, merging the yielding properties of steel with the elastic characteristics of GFRP. Stiffness in SGW1 and SGW2 remained above 14% at 1% drift and decreased gradually to 8.6% and 6.2% at failure. This hybrid response reflects the key role of steel to initial stiffness and ductility, while the GFRP bars enhanced stiffness retention with increasing drift. Although hybrid walls experienced greater stiffness degradation than the GFRP-only walls, they retained more stiffness than the steel-RC walls, particularly after steel yielding.

**Fundamental period shift**

Accurate calculation of the fundamental period of RC structures is essential for seismic assessment, as it directly influences the magnitude of earthquake-induced forces. The fundamental period is largely governed by the structure's mass and effective stiffness, and changes in stiffness due to damage can cause significant shifts in the period [39]. An increase in the fundamental period, resulting from stiffness degradation, typically reduces earthquake forces for structures with a period greater than 0.5 seconds. However, for those with a period below 0.2 seconds, an increase in the period may amplify seismic forces [26].

To appraise the period shift, the fundamental period ($T_B$) was computed as $T_B = 2\pi\sqrt{m/K_s}$, where $m$ represents the reactive mass of an equivalent single-degree-of-freedom (SDOF) system, and $K_s$ is the considered secant stiffness at a specific drift level. With mass constant, period shift calculations relied on $T_i = \sqrt{K_i/K_s}\,T_0$, where $T_0$ denotes the initial period. Table 3 summarizes the calculated period shifts for each wall at various damage stages.

During the initial loading phase, prior to yielding, GFRP-RC walls evinced higher period shifts than steel and hybrid-reinforced walls. At drift levels associated with concrete spalling, period shift reached 1.85 for GW1 and 2.25 for GW2, compared to 1.15 for SW1 and 1.32 for SGW2. This enhanced period shift in GFRP-RC walls can be stemming from the GFRP elastic characteristics that maintain stiffness without yielding. As cracking and spalling progressed, period shifts increased more significantly in steel- and hybrid-reinforced walls due to more pronounced stiffness degradation. At failure, period shifts reached 2.73 in SW1 and 3.22 in SW2, while SGW1 and SGW2 exhibited shifts of 2.65 and 3.15, respectively. Whereas, GFRP-RC walls showed slower increases, with final period shifts of 2.60 for GW1 and 3.06 for GW2.

These findings reflect the close correlation between stiffness degradation along with fundamental period shifts. In steel-reinforced walls, the sharp drop in stiffness post-yielding significantly increases the fundamental period, while in GFRP-RC walls, the gradual degradation of stiffness leads to more moderate period shifts. Hybrid-reinforced walls, benefiting from the complementary properties of steel and GFRP, exhibit intermediate period shifts, balancing the ductility of steel with the elastic resilience of GFRP. This behavior underscores the importance of selecting appropriate reinforcement strategies to optimize both stiffness retention and seismic performance.

**Table 3.** Overview of experimental damage evolution and corresponding fundamental period shift

| Characteristic damage Stage | Wall | $\frac{Q}{Q_u}$% | Δ (mm) | $\frac{T}{T_0}$ |
|---|---|---|---|---|
| Shear Cracking | SW1 | 41.98 | 2.57 | 1.15 |
| | SGW1 | 33.31 | 2.76 | 1.35 |
| | GW1 | 28.29 | 5.16 | 1.85 |
| | SGW2 | 48.42 | 3.27 | 1.32 |
| | GW2 | 45.27 | 3.59 | 1.49 |
| | GW3 | 32.81 | 6.42 | 2.25 |
| Concrete spalling | SW1 | 96.25 | 23.66 | 2.73 |
| | SGW1 | 95.25 | 26.95 | 2.65 |
| | GW1 | 84.11 | 30.13 | 2.60 |
| | SGW2 | 99.23 | 29.00 | 3.22 |
| | GW2 | 98.62 | 31.78 | 3.15 |
| | GW3 | 84.52 | 34.06 | 3.06 |
| Concrete crushing | SW1 | 97.11 | 26.33 | 2.92 |
| | SGW1 | 96.87 | 34.92 | 2.83 |
| | GW1 | 96.67 | 39.33 | 2.77 |
| | SGW2 | 99.23 | 29.00 | 3.47 |
| | GW2 | 99.09 | 33.23 | 3.22 |
| | GW3 | 99.59 | 41.58 | 3.15 |

### 3.4 Idealized displacement ductility

The idealized displacement ductility ($\mu_{\Delta}^{id}$) of each tested squat shear wall was quantified utilizing the equivalent energy elastic-plastic method [21,23]. This approach idealizes the load-drift envelope by approximating the actual nonlinear response with a bilinear curve [26], as presented in Fig. 8. Ductility index was calculated as maximum lateral displacement at failure divided by idealized yield displacement. The idealized backbone curves for all specimens are depicted in Fig. 9, with key parameters summarized in Table 4.

**Table 4.** Obtained parameters of idealized backbone curves for tested walls

| Specimen | Yield Drift (%) | Ultimate Drift (%) | Yield Strength $kN$ | $\mu_{\Delta}^{id}$ |
|---|---|---|---|---|
| SW1 | 0.78 | 2.54 | 580.00 | 1.81 |
| SGW1 | 1.11 | 2.38 | 500.00 | 1.56 |
| GW1 | 1.33 | 2.25 | 430.00 | 1.52 |
| SW2 | 0.69 | 2.68 | 620.00 | 2.03 |
| SGW2 | 0.94 | 2.63 | 600.00 | 1.97 |
| GW2 | 1.44 | 2.30 | 490.00 | 1.30 |

Experimental results indicate that steel-RC walls and hybrid steel-GFRP reinforced walls (SGW1, SGW2) achieved significantly superior displacement ductility relative to GFRP-RC walls. Specifically, $\mu_{\Delta}^{id}$ for steel-RC walls SW1 and SW2 were 1.81 and 2.03, while hybrid walls exhibited values of 1.56 (SGW1) and 1.97 (SGW2). Notably, the enhanced ductility of SGW2, which exceeded the corresponding value for the control wall SW1, can be ascribed to the concentrated steel reinforcement along the wall extremities and the inclusion of boundary confinement. These design features improve confinement in the compression zone, thereby delaying concrete spalling and allowing greater ductility and lateral strength through optimized stress distribution and enhancing the wall's ability to undergo plastic deformations [13,23,24,35]

In contrast, GFRP-RC walls displayed diminished displacement ductility, with $\mu_{\Delta}^{id}$ values of 1.52 and 1.30, respectively. The reduced ductility in these walls is primarily results from the elastic characteristics of GFRP bars, which, unlike steel, do not exhibit yielding or plastic deformation. Instead, GFRP reinforcement undergoes strain-hardening, constraining energy dissipation potential and limiting the ability for significant inelastic displacements prior to failure. Consequently, GFRP-RC walls demonstrated markedly attenuated displacement ductility relative to their steel-reinforced counterparts.

Steel-reinforced walls demonstrated the highest ductility on account of the material's inherent ability to undergo significant plastic deformation, contributing to more gradual post-yield response. Hybrid walls, combining the elastic characteristics of GFRP with the post-yield deformation aptitude of steel, exhibited intermediate ductility values, benefiting from the ductile properties of reinforcement steel in critical regions while maintaining the stiffness advantages of GFRP in the web.

These findings underscore the critical influence of reinforcement type on the ductility of RC squat shear walls. Steel reinforcement provides an enhanced capacity for plastic deformation, leading to increased energy dissipation along with enhanced ductility, making it ideal for seismic applications. In contrast, GFRP-reinforced systems, while offering advantages pertaining to corrosion resistance and stiffness retention, exhibit limited ductility stemming from their limited yielding behavior. Hybrid systems, by combining the strengths of both materials, offer a balanced solution that enhances both ductility, overall performance and resilience of RC squat shear walls under dynamic loading conditions.

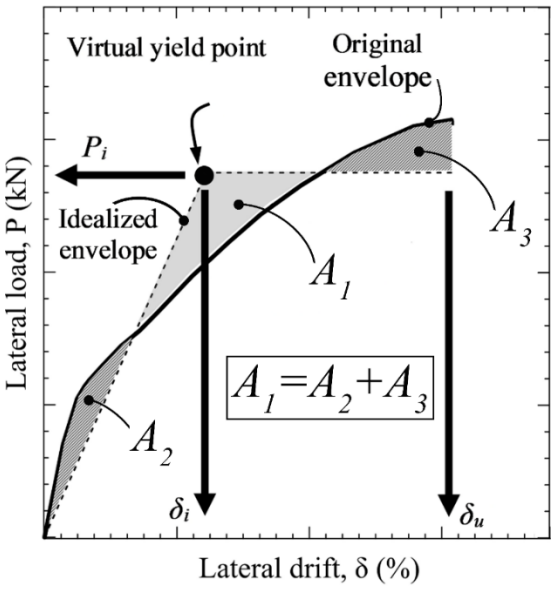


**Fig. 8.** Adopted bilinear idealization of the lateral load-drift envelope, [26]

## 4 Conclusions

The present investigation advances the field of earthquake engineering by providing an in-depth empirical assessment of the seismic behavior of GFRP- and hybrid GFRP/steel-RC squat shear walls. The findings are anticipated to inform the development of future design guidelines for the application of GFRP and hybrid systems in seismically active regions, where structural resilience and long-term durability are paramount. Key performance metrics— including load-carrying capacity, deformation aptitude, stiffness attenuation, and failure mechanisms—were thoroughly evaluated, highlighting the potential of GFRP and hybrid systems to fortify the seismic resilience of squat RC shear walls. Additionally, the study highlights the critical contribution of boundary confinement in reinforcing overall wall integrity and improving shear capacity. The following are the key observations and conclusions drawn from this study:

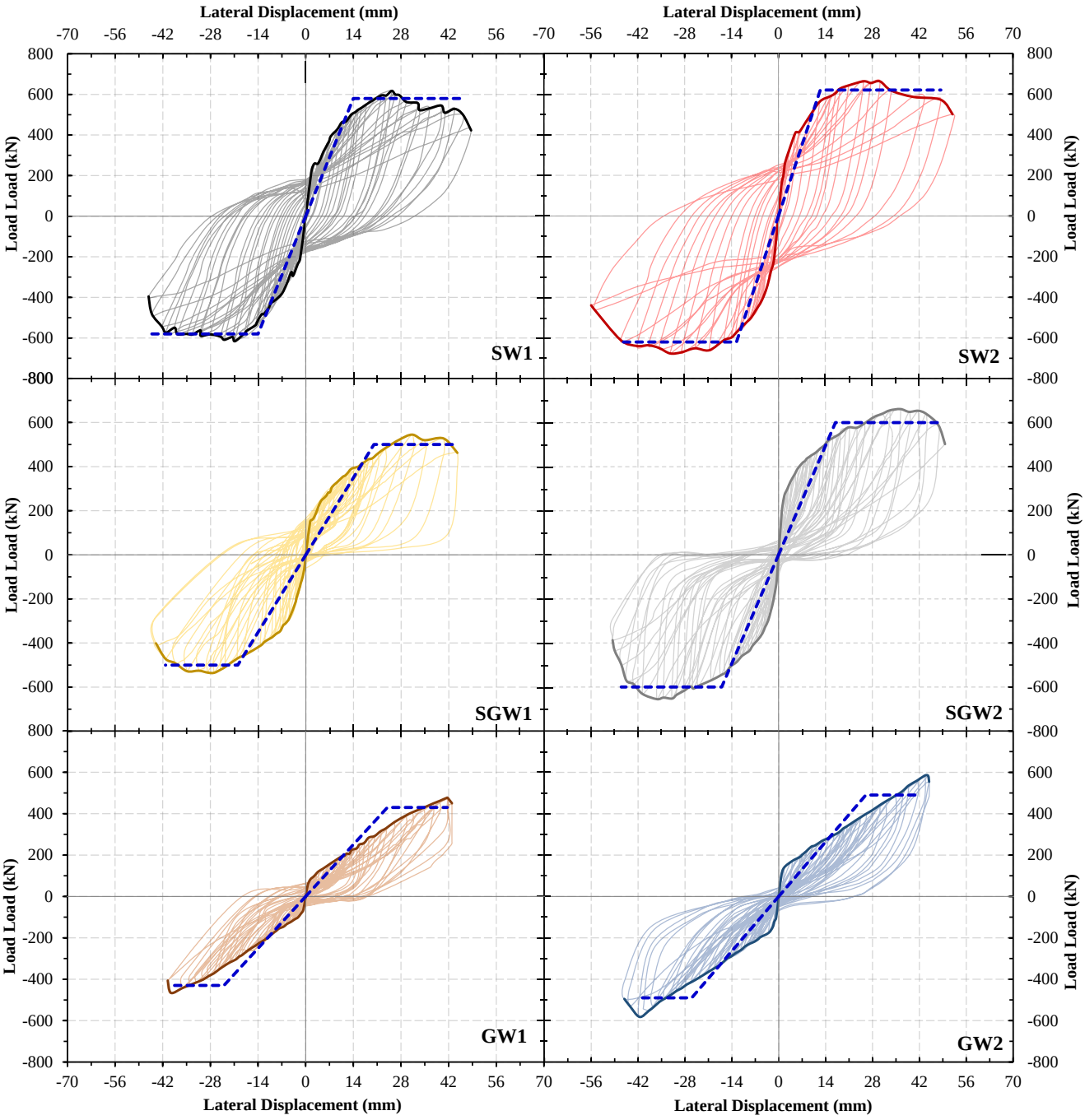


**Fig. 9.** Hysteretic response, backbone curve, and idealized backbone curve for: a) control wall specimen, b & c) hybrid steel-GFRP reinforced walls, and d & e) GFRP-reinforced walls

- Distinct structural responses emerged among the steel-reinforced, GFRP-reinforced, and hybrid-reinforced walls, attributable to the unique material properties and their interactions with the concrete matrix. The comparative analysis of load-displacement envelopes elucidated the significant impact of steel's high yield strength, GFRP's elastic-brittle behavior, and the composite response of hybrid configurations that synergistically harness the advantages of both materials. Of particular significance is the marked improved lateral load resistance exhibited by walls incorporating boundary elements, which effectively confines the compression zone and delays the onset of critical failure modes.
- The progression of cracking and failure modes was markedly influenced by the reinforcement type. Steel-RC walls exhibited well-defined flexural cracks that transitioned into combined shear-

flexural failures with continued loading. GFRP-RC walls, in contrast, displayed brittle cracking behaviors characterized by reduced ductility and a rapid post-peak stiffness decline. Hybrid walls exhibited intermediate responses, with boundary confinement mitigating crack development and preventing premature shear failures.

- Stiffness degradation, evaluated through hysteretic loop analysis, displayed varied trends across reinforcement types. Steel-RC walls manifested significant post-yield stiffness degradation attributable to steel yielding coupled with progressive cracking. Conversely, GFRP-RC walls maintained higher residual stiffness through multiple loading cycles, though at the cost of reduced energy dissipation aptitude. Hybrid walls demonstrated balanced stiffness degradation profiles, benefiting from GFRP's elasticity combined with steel's energy absorption properties.
- Ductility capacity emerged as a critical factor, with idealized ductility indices computed and compared across the wall configurations. Steel-RC walls demonstrated superior ductility, particularly those with boundary elements, which allowed for substantial inelastic deformations before failure. Conversely, GFRP-RC walls evinced limited ductility ascribed to their inherently brittle nature; however, the inclusion of boundary confinement enhanced their overall performance. Hybrid walls effectively combined the ductility of steel with the stiffness of GFRP, yielding moderate ductility indices that affirm their potential as an effective alternative in seismic design.

## References

1. W. Kassem, "Shear strength of squat walls: A strut-and-tie model and closed-form design formula," Engineering Structures, vol. 84 , pp. 430-438, 2015.
2. T. Paulay and M. J. N. Priestley, Seismic design of reinforced concrete and masonry buildings, New York,: John Wiley and Sons Inc., 1992.
3. L. M. Massone, K. Orakcal and J. W. Wallace., "Modeling of Squat Structural Walls Controlled by Shear," ACI Structural Journal, vol. 106, no. 5, pp. 646-655, 2009.
4. N. Time, H. Jang, S. Hwang and J. Jeon, "Data-driven machine-learning-based seismic failure mode identification of reinforced concrete shear walls," Engineering Structures, vol. 208, p. 110331, 2020.
5. C. A. Whyte and B. Stojadinovic, "Effect of Ground Motion Sequence on Response of Squat Reinforced Concrete Shear Walls," Journal of Structural Engineering, vol. 140, no. 8, p. A4014004, 2014.
6. T. Terzioglu, K. Orakcal and L. Massone, "Cyclic lateral load behavior of squat reinforced concrete walls," Engineering Structures, vol. 160, pp. 147-160, 2018.
7. Z. Tuna, Seismic Performance, Modeling, and Failure Assessment of Reinforced Concrete Shear Wall Buildings, Los Angeles: PhD Thesis, University of California, 2012.
8. H. el-Kady, O. Ame, A. Shawky, A. H. Ali and H. Haggag, "Quasi-static Cyclic In-plane Testing of Slender GFRP-Reinforced Concrete Shear Walls," Civil Engineering Beyond Limits, vol. 3, no. 3, p. 1737, 2022c.
9. U. Angst, "Challenges and opportunities in corrosion of steel in concrete," Materials and Structures, vol. 51, pp. 1-20, 2018.
10. L. Bertolini, "Steel corrosion and service life of reinforced concrete structures," Structure and Infrastructure Engineering, vol. 4, pp. 123 - 137, 2008.
11. R. E. Melchers and I. A. Chaves, "Durable Steel-Reinforced Concrete Structures for Marine Environments," Sustainability, vol. 13, no. 24, p. 13695, 2021.
12. C. Jiang, Y. Wu and M. Dai, "Degradation of steel-to-concrete bond due to corrosion," Construction and Building Materials, vol. 158, pp. 1073-1080, 2018.
13. M. El-Gendy and E. El-Salakawy, "Effect of flexural reinforcement type and ratio on the punching behavior of RC slab-column edge connections subjected to reversed-cyclic lateral loads," Engineering Structures, vol. 200, p. 109703, 2019.
14. C. Kassem, A. S. Farghaly and B. Benmokrane, "Evaluation of Flexural Behavior and Serviceability Performance of Concrete Beams Reinforced with FRP Bars," Journal of Composites for Construction, vol. 15, no. 5, pp. 682-695, 2011.

15. C. E. Bakis, L. C. Bank, V. L. Brown, E. Cosenza, J. F. Davalos, J. J. Lesko, A. Machida, S. H. Rizkalla and T. C. Triantafillou, "Fiber-Reinforced Polymer Composites for Construction—State-of-the-Art Review," Journal of Composites for Construction, vol. 6, no. 2, pp. 73-87, 2002.
16. E. El-Salakawy, B. Benmokrane, A. El-Ragaby and D. Nadeau, "Field Investigation on the First Bridge Deck Slab Reinforced with Glass FRP Bars Constructed in Canada," Journal of Composites for Construction, vol. 9, no. 6, pp. 470-479, 2005.
17. M. K. Sharbatdar and M. Saatcioglu, "Seismic Design of FRP Reinforced Concrete Structures," Asian Journal of Applied Sciences, vol. 2, no. 3, pp. 211-222, 2009.
18. H. Tobbi, A. S. Farghaly and B. Benmokrane, "Concrete Columns Reinforced Longitudinally and Transversally with Glass Fiber-Reinforced Polymer Bars," ACI Structural Journal, vol. 109, no. 4, pp. 551-558, 2012.
19. N. Mohamed, A. S. Farghaly, B. Benmokrane and K. W. Neale, "Flexure and Shear Deformation of GFRP-Reinforced Shear Walls," Journal of Composites for Construction, vol. 18, no. 2, p. 04013044, 2014b.
20. Tavassoli, J. Liu and S. Sheikh, "Glass Fiber-Reinforced Polymer-Reinforced Circular Columns under Simulated Seismic Loads," ACI Structural Journal, vol. 112, no. 1, pp. 103-114, 2015.
21. N. Mohamed, A. S. Farghaly, B. Benmokrane and K. W. Neale, "Experimental Investigation of Concrete Shear Walls Reinforced with Glass Fiber–Reinforced Bars under Lateral Cyclic Loading," Journal of Composites for Construction, vol. 18, no. 3, pp. A4014001-1-12, 2014a.
22. Arafa, A. S. Farghaly and B. Benmokrane, "Experimental Behavior of GFRP-Reinforced Concrete Squat Walls Subjected to Simulated Earthquake Load," Journal of Composites for Construction, vol. 22, no. 2, pp. 04018003-1-14, 2018c.
23. H. El-Kady, O. Ame, A. H. Ali and H. Haggag, "Experimental Investigation on the Cyclic In-Plane Behavior of GFRP-Reinforced Concrete Shear Walls," Buildings, vol. 12, no. 11, p. 1948, 2022a.
24. H. el-Kady, O. Amer, A. H. Ali and H. Haggag, "Hysteretic Performance of Hybrid GFRP-Steel Reinforced Concrete Shear Walls: An Experimental Investigation," Journal of Cement Based Composites, vol. 3, no. 4, p. 5736, 2022b.
25. M. Elshamandy, A. Farghaly and B. Benmokrane, "Experimental behavior of glass fiber-reinforced polymer-reinforced concrete columns under lateral cyclic load," ACI Structural Journal, vol. 115, pp. 337-349, 2018.
26. Shabana, A. S. Farghaly and B. Benmokrane, "Earthquake response of GFRP-reinforced concrete squat walls with aspect ratios of 1.14 and 0.68," Engineering Structures, vol. 252 , p. 113556, 2022.
27. B. N. Luna and A. S. Whittaker, "Peak strength of shear-critical reinforced concrete walls," ACI Structural Journal, vol. 116, no. 2, pp. 257-266, 2019.
28. Arafa, A. S. Farghaly and B. Benmokrane, "Effect of web reinforcement on the seismic response of concrete squat walls reinforced with glass-FRP bars," Engineering Structures, vol. 174, pp. 712-723, 2018a.
29. ACI 318, Building code requirements for structural concrete and Commentary (ACI 318-19), Farmington Hills, MI: American Concrete Institute, 2019.
30. ECP 203, Egyptian Code for Design and Construction of Reinforced Concrete Structures, Cairo, Egypt: Ministry of Housing, Utilities and Urban Development - Housing and Building National Research Center, 2021.
31. O. A. El-Azizy, M. T. Shedid, W. W. El-Dakhakhni and R. G. Drysdale, "Experimental evaluation of the seismic performance of reinforced concrete structural walls with different end configurations," Engineering Structures, vol. 101, p. 246–263, 2015.
32. ECP 208, The Egyptian Code of Practice on the Use of Fibre Reinforced Polymers in the Construction Fields, Cairo, Egypt: Ministry of Housing, Utilities and Urban Development - Housing and Building National Research Center, 2005.
33. ACI 440.1R, Guide for the design and construction of structural concrete reinforced with FRP bars, Farmington Hills, MI: American Concrete Institute, 2015.
34. ASTM D7205/D7205M-06, "Standard Test Method for Tensile Properties of Fiber Reinforced Polymer Matrix Composite Bars," ASTM, West Conshohocken, PA, 2011.
35. Z. Huang, J. Shen, H. Lin, X. Song and Y. Yao, "Shear behavior of concrete shear walls with CFRP grids under lateral cyclic loading," Engineering Structures, vol. 211, p. 110422, 2020.
36. Zhao, F. Shen, C. Si, Y. Sun and L. Yin, "Experimental Investigation on Seismic Resistance of RC Shear Walls with CFRP Bars in Boundary Elements," International Journal of Concrete Structures and Materials, vol. 14, pp. 1-20, 2020.

37. Hassanein, N. Mohamed, A. S. Farghaly and B. Benmokrane, "Effect of boundary element confinement configuration on the performance of GFRP-Reinforced concrete shear walls," Engineering Structures, vol. 225, p. 111262, 2020b.
38. Arafa, A. S. Farghaly and B. Benmokrane, "Evaluation of Flexural and Shear Stiffness of Concrete Squat Walls Reinforced with Glass Fiber-Reinforced Polymer Bars," ACI Structural Journal, vol. 115, no. 1, pp. 211-221, 2018b.
39. M. Hadzima-Nyarko, H. Draganić, H. Draganić and T. Štefić, "Comparison of fundamental periods of reinforced shear wall dominant building models with empirical expressions," Tehnički vjesnik, vol. 22, no. 3, pp. 685-694, 2015.